IEEE Access
Multidisciplinary | Rapid Review | Open Access Journal

Received 25 July 2024, accepted 1 August 2024, date of publication 5 August 2024, date of current version 15 August 2024.

Digital Object Identifier 10.1109/ACCESS.2024.3438790

RESEARCH ARTICLE

A Heuristic Forward Scatter Radar Detector for Sky Fence With Opportunistic Signals From LEO Satellites

DEFENG HUANG, (Senior Member, IEEE)
Department of Electrical, Electronic, and Computer Engineering, The University of Western Australia, Perth, WA 6009, Australia
e-mail: david.huang@uwa.edu.au

This work was supported in part by Australian Research Council Discovery Project under Grant DP220101894.

ABSTRACT Traditionally, the crystal video detector (CVD) has been used in a forward scatter (FS) radar to detect a moving target, with the requirement that some parameters of the target, such as its shape and locations, are available *a priori*. This work introduces a simple heuristic detector based on the variance changes in received signal amplitudes, eliminating the need for target parameters. The proposed detector is suitable for ground-based FS radars using opportunistic signals from broadband low Earth orbit (LEO) satellite communication systems, particularly for unmanned aerial vehicle (UAV) detection in a ''sky fence'' setup. Theoretical analysis of the receiver operating characteristics (ROC) indicates that although the CVD generally outperforms the heuristic detector, the performance gap is minimal with relatively small target-induced Doppler shifts compared with the signal bandwidth of the satellite communication system. Both detectors are effective for small target detection within the narrow beamwidth of antennas used in broadband LEO satellite communications. The proposed detector's application in a simplistic sky fence scenario demonstrates its potential for UAV detection.

INDEX TERMS Low Earth orbit satellites, microwave propagation, passive microwave remote sensing.

I. INTRODUCTION

The proliferation of flying objects due to the emergence of advanced air mobility [1], [2], such as unmanned aerial vehicles (UAVs or drones) and electric vertical takeoff and landing (eVTOL) aircrafts, poses a challenge for air traffic surveillance, particularly the detection of such objects. For example, similar to the way that police radars detect speeding violations on roads, there is a need for technology to ensure compliance with the International Civil Aviation Organization (ICAO) geofencing requirements [3], [4], which dictate specific virtual three-dimensional boundaries of airspace where each aircraft can or cannot fly within during designated time intervals. Current methods for uncooperative flying objects detection include backscatter radars, acoustic receivers, visible/infrared cameras, and RF sensing [5], [6], but cost-effective solutions are still not available.

The associate editor coordinating the review of this manuscript and approving it for publication was Hayder Al-Hraishawi.

Bi-static forward scatter (FS) radars have been widely investigated since seven decades ago [7]. By exploiting various opportunistic signals including those from GNSS [8], terrestrial broadcasting [9], DVB-S [10], ground based passive FS radars have recently attracted a lot of attention for their capability in air object detection. Using opportunistic signals from satellites, CubeSat-based FS passive radars have also been proposed for space debris detection [11].

Along with the deployment of low Earth orbit (LEO) satellite megaconstellations for global Internet services (e.g. Starlink), an increasing number of LEO satellites beam down microwave signals from space. Recently we have proposed to opportunistically use those signals as the source of the ground based passive FS radars for flying target detection [12], [13]. Particularly, the Doppler effect has been analyzed in [12] and a positioning method using the amplitudes of the received signals from multiple ground stations was presented in [13].

By utilizing the ground based FS passive radars, in this work we will investigate the use of a sky fence for the

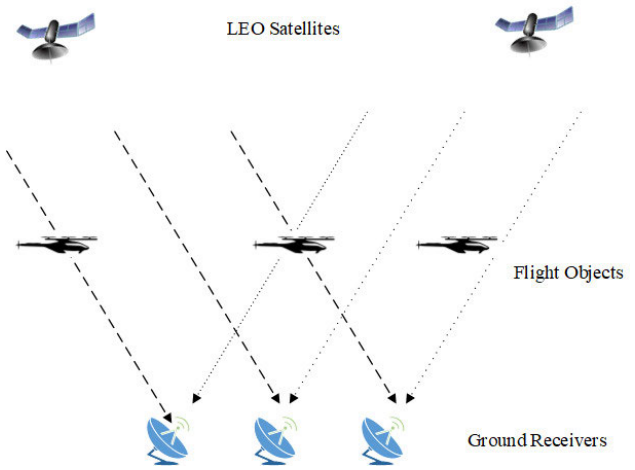

FIGURE 1. 2D depiction of the envisioned sky fence.

detection of UAVs, i.e., a network of microwave links connecting multiple LEO satellites to multiple ground-based receivers across diverse locations, as shown in Fig. 1. The concept of utilizing a fence of microwave links for object detection dates back to 1934 when an FS radar fence was tested for marine target detection [7]. Recently the network of ground-based FS radars proposed in [15] and [16] can be treated as a sky fence. Beyond FS radars, in 2020, the US$1.5 billion space fence project in the Marshall Islands was commissioned to surveil space objects [17], [18], which utilizes back-scattered radars with narrow beams generated by large phased-array antennas.

The sky fence envisioned has distinct advantages for UAV detection: it leverages opportunistic microwave signals for Internet services from existing LEO satellites, thereby without additional cost for air traffic surveillance; by potentially utilizing off-the-shelf components, the ground receivers are cheap due to economy of scale, thereby facilitating cost-effective large-scale deployment; it is immune to stealth technology due to the attributes of the FS region [14].

Most previous analytical work on passive FS radars, such as [15] and [16], was based on radar cross section (RCS), which, under the context of FS radars, is also known as forward scatter cross section [19]. To utilize the RCS, the direct signal from the passive source must be available at the receiver, which is often unrealistic [20], particularly if the source is from LEO satellites. To avoid the requirement of the direct signal retrieval, the crystal video detector (CVD) [21] or its variants [22] are often employed at the receiver, which use an amplitude detector to retrieve the scattered signal by exploiting the relative movement between the target and the link between the transmitter and the receiver. However, to use the CVD or its variants, all or some parameters of the moving target need to be available or through the trials of different values of the parameters - a challenging task for the UAV detection, given the diverse range of UAV types and the risk of overfitting. Furthermore, previous coverage analysis with the RCS was based on one observation point [15], [16], rather than multiple observation points (or a continuous time span of observations) as required by the CVD. Finally, no prior work on passive FS radars has delved into the intricacies of communication systems, such as the effects of communication signals and the beam-width of the receive antenna.

In this work, by utilizing the difference in the variances of the amplitude when a target is present or not, a simple heuristic detector is proposed for FS radars with opportunistic signals from LEO satellites. The test statistics of the detector is the standard deviation of the amplitude with the best straight-line fit removed to eliminate the impact of the continuing movement of the LEO satellite. Compared with the CVD or its variants [21], [22], the proposed detector does not require the availability of the target's parameters, thereby much simpler. In general the amplitude of the received signal at the ground station is a nonlinear mixture of the signal and the noise. However, we will show that if the direct signal to noise ratio (DNR) is relatively large and the target's disturbance to the signal is relatively small, then the amplitude can be approximated as a signal term plus a noise term. With the approximation, the receiver operating characteristic (ROC) is derived for opportunistic communication signals with single tone signals as a special case. It will be shown that the analytical ROC results are very close to the simulation results for both constant amplitude modulation (e.g. QPSK [26]) and non-constant amplitude modulation (e.g. 16QAM [26]).

With the amplitude approximated as a signal term plus a noise term, it will also be shown that the ROC of the CVD can be easily obtained. The ROC performance of the heuristic detector improves along with the increase of the number of independent samples to estimate each amplitude of the received signal, while that of the CVD is not related to the number of independent samples. In general the ROC performance of the CVD is better than that of the proposed heuristic detector. However, the ROC performance of the heuristic detector is comparable with that of the CVD if the number of independent samples are large, which is often the case for broadband LEO satellite communication systems, as the target-induced Doppler shifts are small compared with the signal bandwidth.

For passive FS radars exploiting opportunistic signals from LEO satellites such as the Starlink constellation, the ground receive antenna needs to be always directed at the LEO satellite, and only a target within the beamwidth of the antenna is of practical interest. The beamwidth of the receive antenna for broadband satellite communications is often narrow. For a small target moving within the narrow beamwidth of a few degrees, it will be shown that the proposed heuristic detector can achieve very high probability of detection, same as the CVD.[1] The probability of detection for a small target crossing multiple links of a sky fence is then analyzed for a simplistic scenario to gain insights. It will

[1]A narrow antenna beamwidth also reduces clutters, the disussion of which is out of scope of this paper.

be shown that, with the distance between adjacent ground stations about 1,500 meters, a probability of detection about 50 percent can be achieved for detecting a small target of about 500 meters height, if the target crosses about 34 links. By contrast, for Starlink, the number of LEO satellites within the line of sight of a ground station above the minimum required satellite elevation angle is more than 20 for most places on the Earth, and the beacon signals (i.e., single tone signals for tracking Doppler frequency of LEO satellites) are often available for use [23], [27].

This paper is an extended version of our recent conference publication [30]. Compared to [30], the following additions have been made:

1) *ROC Theoretical Analysis*: This paper includes a comprehensive theoretical analysis of the ROC.
2) *Sky Fence Concept*: This paper introduces the concept of the sky fence and analyze its capability in detecting small flight targets.
3) *Receive Antenna Beamwidth*: The impact of receive antenna beamwidth on the probability of detection is examined in this paper.
4) *Simulation Scenarios*: Simulations of small flying targets at heights of 100m and 500m are presented, whereas the previous study [30] focused on large airplanes at a height of 10,000m.

This paper is organized as follows. The FS radar system model for opportunistic communication signals from LEO satellites is introduced in Section II. The heuristic variance based detector is proposed in Section III. The ROCs for both the proposed heuristic detector and the CVD are derived in Section IV. Numerical results are presented in Section V, and conclusion is drawn in Section VI.

II. SYSTEM MODEL

A. SINGLE TONE SIGNAL

As in [12], a rotational Cartesian coordinate system (x, y, z) of Fig. 2 is used. The ground receiver is located at the origin. The x axis is parallel to the ground plane, and the y axis is along the link[2] between the LEO satellite and the ground receiver, which rotates around the ground receiver. Let $y_S(t)$ denote the distance between the satellite and the ground receiver. Then the coordinate of the satellite is $(0, y_S(t), 0)$. (x', y', z') is another rotational Cartesian coordinate system with the origin

[2]For the purpose of this work the ground receiver does not need to communicate with the satellite. However, the satellite must beam down a signal and the ground receiver must fall within the beam of the satellite, which often covers a range of at least tens of kilometers.

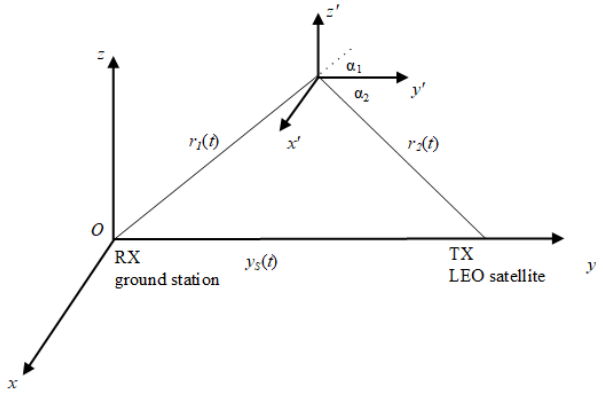

FIGURE 2. Coordinates for the system model.

attached to the centroid of the target and the (x', y', z') axes are parallel with the (x, y, z) axes, respectively.

Using the Fresnel-Kirchhoff diffraction formula and Babinet's principle [24], the complex amplitude of the received signal at the ground station is given by (1), as shown at the bottom of the page. In (1), $n(t) = n_I(t) + jn_Q(t)$ is the additive white Gaussian noise (AWGN). Let the variance of $n(t)$ be $\sigma_n^2 \equiv E(n(t)n^*(t))$, where $E(\cdot)$ is the expectation of $(\cdot)$ and $(\cdot)^*$ is the conjugate of $(\cdot)$. Then the variance of $n_I(t)$ and that of $n_Q(t)$ are given by $\sigma_{n_I}^2 = \sigma_{n_Q}^2 = \frac{\sigma_n^2}{2}$. In (1), A_s is the complex amplitude of a single tone signal at the satellite transmitter, the wave number $k = 2\pi/\lambda$, where λ is the wavelength, the diffraction angles α_1 and α_2 are both approximated as 0, and

$$F(x', z') = \begin{cases} 1, & \{x', z'\} \in \Sigma \\ 0, & otherwise \end{cases}$$

where Σ is the 2D image of the target projected onto the $x' - z'$ plane. Note that here we assume that the thickness of the target in the y' direction is negligible. Also note that (1) is a baseband equivalent model, thereby the Doppler shift of the carrier of the communication signals due to the movement of the LEO satellite only, which can be known *a priori* [25], is assumed to having been perfectly compensated for. Let the coordinate of the centroid of the target at time t under the (x, y, z) coordinate be $(x_F(t), y_F(t), z_F(t))$. Then the distance between a point $(x', 0, z')$ on the target and the ground receiver, and that between the point and the satellite are given by

$$r_1 = \sqrt{(x_F(t) + x')^2 + y_F^2(t) + (z_F(t) + z')^2}$$

$$\begin{aligned} U(t) &= \frac{A_s e^{jky_S(t)}}{y_S(t)} - \frac{A_s}{j2\lambda} \int\int F(x', z') \frac{e^{jk(r_1+r_2)}}{r_1 r_2} (cos\alpha_1 + cos\alpha_2) dx' dz' + n(t) \\ &\approx \frac{A_s e^{jky_S(t)}}{y_S(t)} + \frac{jA_s}{\lambda} \int\int F(x', z') \frac{e^{jk(r_1+r_2)}}{r_1 r_2} dx' dz' + n(t). \end{aligned} \tag{1}$$

$$U(t) = \frac{A(t)}{y_S(t)} e^{j\varphi(t)} \left[1 + y_S(t) \int\int A_{x',z'}(t) e^{j\varphi_{x',z'}(t)} dx' dz' \right] + n(t). \tag{2}$$

and

$$r_2 = \sqrt{\left(x_F(t) + x'\right)^2 + \left(y_F(t) - y_S(t)\right)^2 + \left(z_F(t) + z'\right)^2},$$

respectively.

B. COMMUNICATION SIGNAL

The complex amplitude of a communication signal is not a constant in time, thereby $A_s e^{jky_S(t)}$ in (1) needs to be replaced with a time-variant complex-valued random variable $A(t)e^{j\varphi(t)}$, where $A(t)$ and $\varphi(t)$ are the amplitude and the phase of the communication signal, respectively. Then the system model (1) becomes (2), as shown at the bottom of the previous page. In (2), $A_{x',z'}(t)$ and $\varphi_{x',z'}(t)$ are the amplitude and the phase induced by point (x', z') on the flying object, respectively. The direct signal to noise power ratio is then defined as follows.

$$DNR = \frac{E\left(\frac{A^2(t)}{y_S^2(t)}\right)}{\sigma_n^2}. \tag{5}$$

Let the amplitude of $U(t)$ be $S_A(t)$. For relative high DNR and small $A_{x',z'}(t)$, similar to the noise performance analysis of the envelope detection with the phasor diagram representation [26], from (2), $S_A(t)$ can be approximated by (6), as shown at the bottom of the next page. In (6), $Re[\cdot]$ is the real component of $[\cdot]$.

Let $n_e(t)$ denote the noise term in (6) as follows.

$$\begin{aligned} n_e(t) &= Re[n(t)e^{-j\varphi(t)}] \\ &= n_I(t)cos(\varphi(t)) + n_Q(t)sin(\varphi(t)). \end{aligned}$$

The variance of $n_e(t)$ is then given by

$$\sigma_{n_e}^2 = \frac{\sigma_{n_I}^2}{2} + \frac{\sigma_{n_Q}^2}{2} = \frac{\sigma_n^2}{2}.$$

Let $A'(t) = A(t) - A$, where A is the expectation of the amplitude $A(t)$. Then (6) becomes (7), as shown at the bottom of the next page. As an example, for a modulation scheme with a constant amplitude such as the M-ary phase shift keying (MPSK) [26], and similarly for a single tone signal, $A'(t) = 0$. For a modulation scheme with a non-constant amplitude such as the quadrature amplitude modulation (QAM), $A'(t) \neq 0$. However, for high data rate communication systems, $A'(t)$, the degree of time-variation of which is proportional to the bandwidth of the communication signal, changes much faster than $A_{x',z'}(t)$ and $\varphi_{x',z'}(t)$, the degree of time-variation of which is proportional to the Doppler shift incurred by the target. For example, the maximum Doppler shift due to a target in the sky is about a few thousand Hertz [12]. By contrast, the bandwidth of the Starlink downlink signal is 240 MHz [27]. Assume that $\int\int A_{x',z'}(t)cos(\varphi_{x',z'}(t))dx'dz'$ is approximately a constant within a time duration of T_A. By averaging $S_A(t)$ over the duration of T_A (alternatively, a low pass filter with a proper bandwidth may be applied), the third term in (7) can be omitted as it is significantly smaller than the second term, due to the fact that most of the power of $A'(t)$ is out of the bandwidth of $\int\int A_{x',z'}(t)cos(\varphi_{x',z'}(t))dx'dz'$. After omitting the third term in (7), the received signal becomes $S_A(t)$ of (3), as shown at the bottom of the page, where $n_I(t)$ and $\dot{A}(t)$ are the averaging of $n_e(t)$ and $A'(t)$, respectively.

Assume that the variance of $A'(t)$ is σ_A^2, and that over the duration of T_A, N_A independent samples can be used. As a result, after an averaging operation over the duration of T_A, the variance of the $\frac{\dot{A}(t)}{y_S(t)} + n_I(t)$ term is equal to $\frac{1}{N_A}\left(\frac{\sigma_A^2}{y_S^2(t)} + \frac{\sigma_n^2}{2}\right)$, and $S_A(t)$ in (3) becomes $S_o(t)$ in (4), as shown at the bottom of the page, where $n_{Total}(t)$ is an Gaussian random variable with variance $\sigma_{total}^2 = \frac{1}{N_A}\left(\frac{\sigma_A^2}{y_S^2(t)} + \frac{\sigma_n^2}{2}\right)$.

III. A SIMPLE VARIANCE BASED DETECTOR

With the simulation setup of Sections V-A and V-B, Figs. 3a to 3c show three examples of the amplitude at the ground receiver for a single tone transmitted from a LEO satellite for a rectangular target of 8.1 meters by 6.4 meters flying in a speed of 100.1 m/s at a height of 500.1 meters and satellite elevation angle $\theta(t = 0) = 40^o, 65^o$ and 90^o, respectively. The minimum distance between the target and the link between the satellite and the ground receiver is 20.1 meters. Corresponding to Figs. 3a to 3c, using the Doppler analysis in [12], the Doppler shifts and Doppler bounds are shown in Figs. 3d to 3f, respectively. It can be seen that due to the moving target, the amplitude of the received signal varies significantly in time. On the other hand, the direct signal (i.e., the first term in (4), $\frac{A}{y_S(t)}$) is also time-variant due to the continuing movement of the LEO satellite.

For a short time, the direct signal can be approximated by a linear function of time, and may be removed, leading to $S(t)$, which is produced by removing the best straight-line linear fit from $S_o(t)$ in (4). As an example, the curve in Fig. 3g is the linear detrend of the amplitude of the received single tone signal in Fig. 3a with Matlab's 'detrend' function. Figs. 3h and 3i are the linear detrend of the amplitude of the received 16QAM communication signals under noisy environment ($DNR = 10dB$) averaged

$$S_A(t) \approx \frac{A}{y_S(t)} + \frac{\dot{A}(t)}{y_S(t)} + A\int\int A_{x',z'}(t)cos\left(\varphi_{x',z'}(t)\right)dx'dz' + n_I(t). \tag{3}$$

$$S_o(t) \approx \frac{A}{y_S(t)} + A\int\int A_{x',z'}(t)cos\left(\varphi_{x',z'}(t)\right)dx'dz' + n_{Total}(t). \tag{4}$$

over $N_A = 100,000$ data symbols with the received signals computed directly by (1) and approximated by (4), respectively.

With $S(t)$, detecting a target becomes an attempt to distinguish between the following hypotheses:

$$\begin{cases} \mathcal{H}_0: & S(t) \approx n_{Total}(t) \\ \mathcal{H}_1: & S(t) \approx O(t) + n_{Total}(t) \end{cases} \tag{8}$$

where $O(t) \approx A \int\int A_{x',z'}(t) cos\left(\varphi_{x',z'}(t)\right) dx'dz'$.

Based on (8), a matched filter may be applied, which, as shown in Section IV-B, is equivalent to the CVD. However, the use of a matched filter requires $O(t)$ to be available at the detector, and to compute $O(t)$, the shape of the target and its locations need to be available *a priori*.[3] Alternatively, some sophisticated detector such as the generalized likelihood ratio test (GLRT) [28] may be used. However, a GLRT detector would require the modeling of the signal term $O(t)$ be very accurate.

In this work, we propose a simple heuristic detector by exploiting the difference of the variances of the received signal when the target is present or not, as follows.

We use the standard deviation of $S(t)$ over a duration of D as the test statistic:

$$T = \sigma_D(S(t)) \equiv \sqrt{\frac{\sum_{n=1}^{N_D} S^2(n)}{N_D}} \tag{9}$$

where $S(n), n = 1, \ldots, N_D$ are independent samples of $S(t)$ over the duration of D, respectively, and N_D is the number of samples employed.

The detector is as follows. If T is greater than a threshold, then it is determined that the target is present; otherwise, the target is determined not present.

IV. RECEIVER OPERATING CHARACTERISTIC

A. VARIANCE BASED DETECTOR

From (9), under $\mathcal{H}_0$, $\frac{\sqrt{N_D}\sigma_D(S(t))}{\sigma_{total}}$ follows chi distribution with N_D degrees of freedom. As a result, the cumulative distribution function (cdf) of $\sigma_D(S(t))$ is given by

$$\begin{aligned} F_{\mathcal{H}_0}(x; N_D) &\equiv Prob(T < x; \mathcal{H}_0) \\ &= F_{\chi^2}\left(\frac{N_D x^2}{\sigma_{total}^2}; N_D\right), \quad \text{for } x > 0 \end{aligned} \tag{10}$$

[3]Note that $O(t)$ is equal to the third term in (3) that was derived from the second term in (1), which is related to the shape of the target and its locations.

where $F_{\chi^2}(x; N_D)$ is the cdf of chi-squared distribution with N_D degree of freedom.

Under $\mathcal{H}_1$, $\frac{\sqrt{N_D}\sigma_D(S(t))}{\sigma_{total}}$ follows non-central chi distribution with N_D degrees of freedom (also called generalized Rayleigh distribution). As a result, the cdf of $\sigma_D(S(t))$ is given by

$$\begin{aligned} F_{\mathcal{H}_1}(x; N_D) &\equiv Prob(T < x; \mathcal{H}_1) \\ &= F_{\chi^2}\left(\frac{N_D x^2}{\sigma_{total}^2}; N_D, \lambda\right), \quad \text{for } x > 0 \end{aligned} \tag{11}$$

where $F_{\chi^2}(x; N_D, \lambda)$ is the cdf of non-central chi-squared distribution with N_D degrees of freedom and the non-centrality parameter λ is given by

$$\lambda = \frac{\sum_{n=1}^{N_D} O(n)^2}{\sigma_{total}^2}.$$

From (10) and (11), we have the ROC, i.e., the relationship between the probability of detection P_D and the probability of false alarm P_{fa}, as follows.

$$\begin{aligned} P_D &= 1 - F_{\mathcal{H}_1}\left(F_{\mathcal{H}_0}^{-1}(1 - P_{fa}; N_D); N_D\right) \\ &= 1 - F_{\chi^2}\left(F_{\chi^2}^{-1}(1 - P_{fa}; N_D); N_D, \lambda\right), \end{aligned} \tag{12}$$

where $(\cdot)^{-1}$ is the inverse function of $(\cdot)$.

B. CRYSTAL VIDEO DETECTOR

If $O(t)$ is known, then a matched filter can be applied to $S(t)$, and the test statistics is given by

$$T_{CVD} = \frac{1}{N_D} \sum_{n=1}^{N_D} O(n) S(n).$$

As shown in the Appendix, the ROC of such a detector is the same as that of the CVD, which can be easily derived as follows.

$$P_D = Q\left(Q^{-1}(P_{fa}) - \sqrt{\lambda}\right), \tag{13}$$

where $Q(x) = \frac{1}{\sqrt{2\pi}} \int_x^\infty e^{-\frac{t^2}{2}} dt$ is the Q-function.

V. NUMERICAL RESULTS

A. SIMULATION SETUP

A LEO satellite with a circular orbit of height $550km$ is assumed to be vertically above the ground station when passing over. $\lambda = 1\ cm$ (i.e. $f_c = 30GHz$). The target is modeled by a rectangular slab with width a meters and length b meters. Let (x, y_G, z_G) be a Cartesian coordinate system

$$S_A(t) = |U(t)| \approx \frac{A(t)}{y_S(t)} + A(t) \int\int A_{x',z'}(t) cos\left(\varphi_{x',z'}(t)\right) dx'dz' + Re\left[n(t)e^{-j\varphi(t)}\right]. \tag{6}$$

$$S_A(t) = \frac{A + A'(t)}{y_S(t)} + A \int\int A_{x',z'}(t) cos\left(\varphi_{x',z'}(t)\right) dx'dz' + A'(t) \int\int A_{x',z'}(t) cos\left(\varphi_{x',z'}(t)\right) dx'dz' + n_e(t). \tag{7}$$

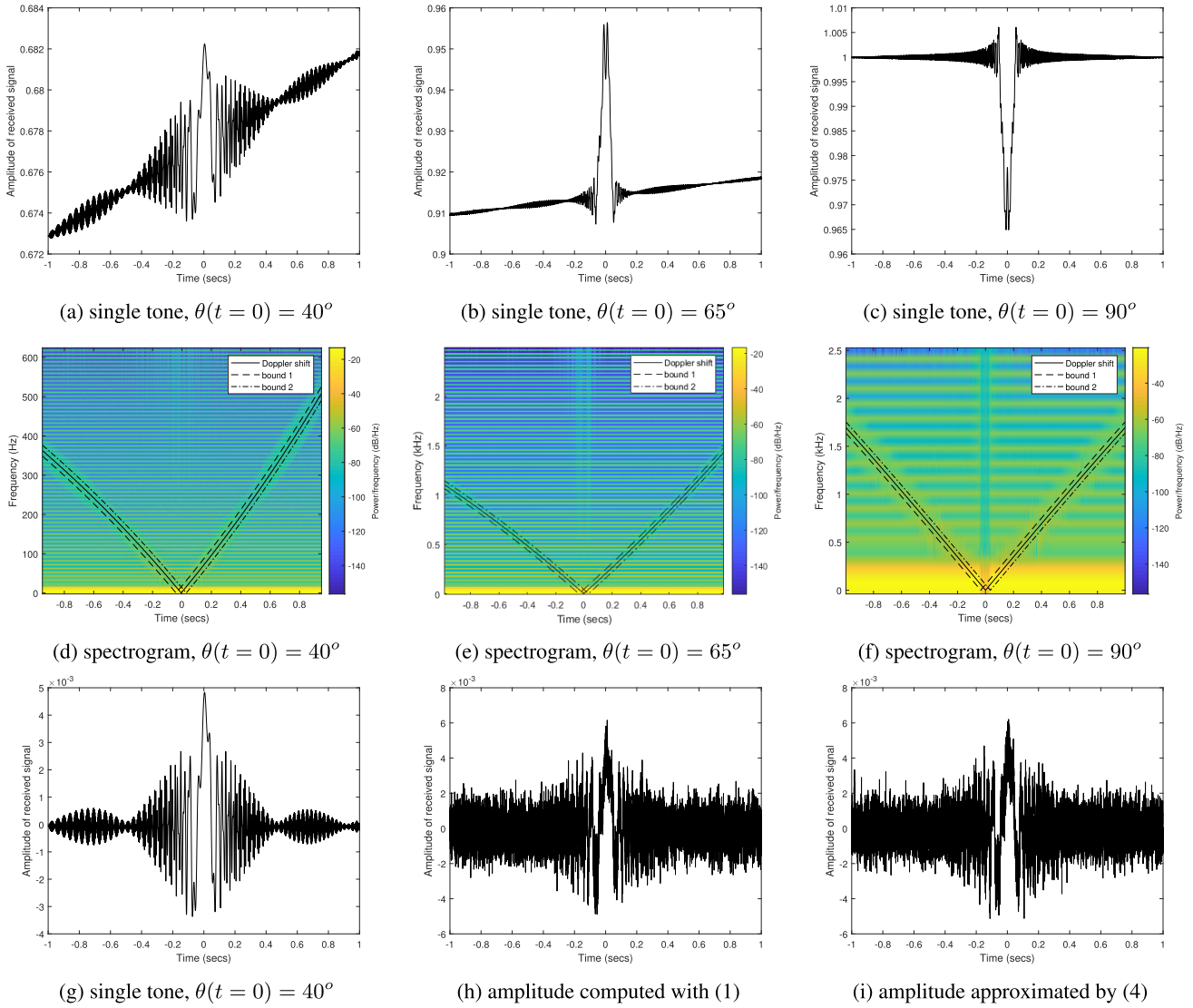

(a) single tone, $\theta(t=0)=40^o$ (b) single tone, $\theta(t=0)=65^o$ (c) single tone, $\theta(t=0)=90^o$

(d) spectrogram, $\theta(t=0)=40^o$ (e) spectrogram, $\theta(t=0)=65^o$ (f) spectrogram, $\theta(t=0)=90^o$

(g) single tone, $\theta(t=0)=40^o$ (h) amplitude computed with (1) (i) amplitude approximated by (4)

FIGURE 3. Received signal at ground station for a rectangular target ($a = 8.1m$, $b = 6.4m$) flying along a straight line ($z_G = 500.1m$, $v_{y_G} = 100.1m/s$, $x = 20.1m$). Figs. 3h and 3i are for communication signals (16QAM) with $N_A = 100,000$, $DNR = 10dB$, and $\theta(t=0) = 40^o$.

fixed on the ground with the $x - y_G$ plane being the ground and the x axis and the origin being the same as those in the rotational coordinate (x, y, z). The coordinate transformation from (x, y_G, z_G) to (x, y, z) is the same as that in [12]. The target flies along the y_G direction with a constant height of h meters above the ground (i.e. $z_G = h$ meters). A positive speed (i.e. $v_{y_G} > 0$) indicates that the target and the satellite move in the same direction, and a negative speed indicates that they are in the opposite direction. The track of the target is assumed to be always parallel with the ground, and its width is in the x direction and its length in the y_G direction. As a result, at time t, the length of the image of the flying object projected onto the xOz plane in the z direction is $bsin(\theta(t))$, where $\theta(t)$ is the elevation angle of the satellite. At $t = 0$, the target is assumed to be just across the link between the satellite and the ground receiver (i.e. the z coordinate of the centroid of the target is equal to zero at $t = 0$). Note that the absolute value of the x coordinate of the centroid of the target (i.e., $|x|$) is equal to the minimum distance between the target and the communication link.

B. RECEIVER OPERATING CHARACTERISTICS

In this section, the ROCs for a rectangular target with width $a = 8.1$ meters and length $b = 6.4$ meters flying at the height of $z_G = 500.1m$ with $v_{y_G} = 100.1m/s$ at a satellite elevation angle $\theta(t = 0) = 65^o$ will be investigated. The duration of observation is 0.4 second (i.e., from -0.2s to 0.2s in Fig. 3b). The target flying along the line of $(x = 20.1m, z_G = 500.1m)$.

Fig. 4 shows the numerical ROC results of (12) for both QPSK (or a single tone signal) and 16QAM in comparison with those directly simulated by (1) (i.e. $S_o(t)$ and $S(t)$ in the

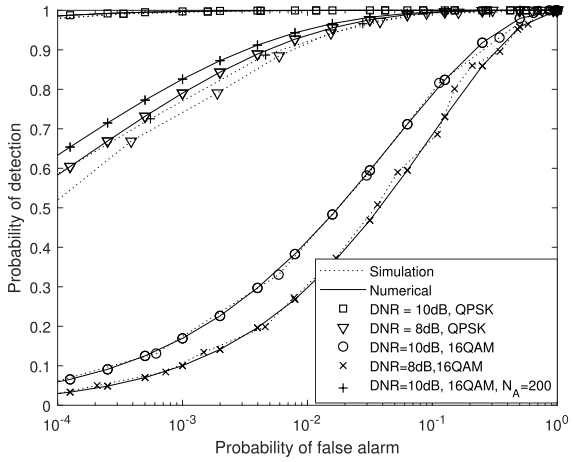

FIGURE 4. ROCs for QPSK (or single tone) and 16QAM for a rectangular target ($a = 8.1m$, $b = 6.4m$) flying along a straight line ($z_G = 500.1m$, $v_{y_G} = 100.1m/s$, $x = 20.1m$, $\theta(t = 0) = 65^o$, $DNR = 8dB$, $10dB$). $N_A = 100$ unless otherwise stated.

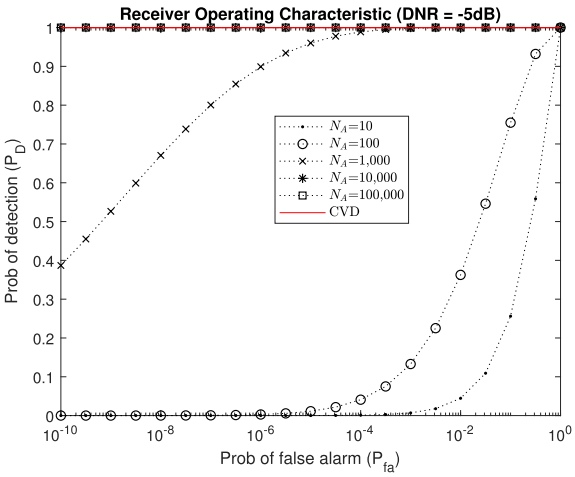

FIGURE 5. ROCs for a rectangular target ($a = 8.1m$, $b = 6.4m$) flying along a straight line ($z_G = 500.1m$, $v_{y_G} = 100.1m/s$, $x = 20.1m$, $\theta(t = 0) = 65^o$, $DNR = -5dB$, 16QAM). The ROC of the heuristic detector and the CVD are computed by (12) and (13), respectively.

test statistics T are replaced with $|U(t)|$ and its linear detrend, respectively). It can be seen that the numerical ROC results of (12) and those directly simulated by (1) are close.

The impact of N_A on the ROC performance is investigated with $N_A N_D = 8,000,000$ kept as a constant. Particularly, N_D samples are uniformly sampled from the 0.4 second time window of the amplitude of the received signals. It can be seen from Fig. 5 that the ROC performance of the heuristic detector improves along with the increase of N_A, while the value of N_A has no impact on the CVD. When N_A is large, the ROC performance of the heuristic detector approaches that of the CVD. This is not surprising as, if the amplitude of the N_A samples is a constant, the averaging operation of N_A samples is equivalent to applying a matched filter. Note that to make it valid that the amplitude of N_A samples is a constant, N_A should be no more than the signal bandwidth divided by N_D, while N_D should be greater than the product of the time window and the maximum Doppler shift incurred by the target.

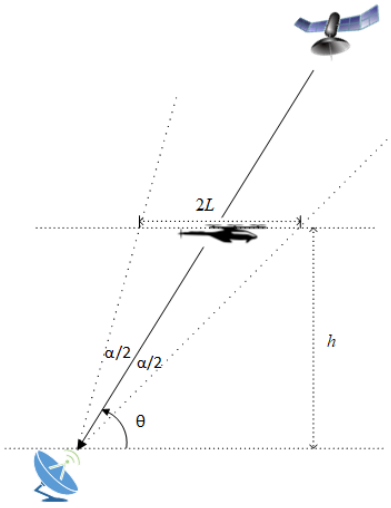

FIGURE 6. Receive antenna beamwidth versus coverage range.

C. RECEIVE ANTENNA BEAMWIDTH

As shown in Fig. 6, the range covered by a ground receive antenna with a narrow beamwidth of α is approximately given by

$$L = \frac{1}{2}\left(\frac{h}{tan(\theta - \frac{\alpha}{2})} - \frac{h}{tan(\theta + \frac{\alpha}{2})}\right) \approx \frac{h\alpha}{2sin^2\theta} \tag{14}$$

where θ is the elevation angle of the satellite.

From (14), Fig. 7 shows the coverage range versus beamwidth at a satellite elevation angle of $\theta = 65^o$, for a target height of 100m, 200m, 500m and 1,000m. For broadband satellite communications, the antenna beamwidth is in general narrow, e.g., about 3.5^o for Starlink. Fig. 7 shows that for a beamwidth of about 3.5^o, the coverage range for a target height of 100 meters and 500 meters is about 3.7 meters and 18.6 meters, respectively.

To investigate the detection capability of the detectors versus the minimum distance (i.e., $|x|$) between the target and the communication link, a duration of 0.4 second of $O(t)$ in (8) was first generated for a small rectangular target ($a = 0.81m$, $b = 0.64m$) flying along a straight line ($(x, z_G = 500m)$, $v_{y_G} = 20\ m/s$, $\theta(t = 0) = 65^o$), for x from 0 to 100 meters. For a probability of false alarm of 10^{-9}, $DNR = 10dB$ and $N_A = 100,000$, Fig. 8 shows that both the heuristic detector and the CVD can successfully detect the target as far as about 30 meters, and both detectors cover a range that is beyond the 3.5^o beamwidth receive antenna. With the same setup as that for Fig. 8 except $v_{y_G} = -20m/s$ (i.e., the target and the satellite fly in the opposite direction), Fig. 9 shows similar results. For a target height of $z_G = 100m$, Fig. 10 shows that both the heuristic detector and the CVD can successfully detect a small target of $a = 0.16m$ and

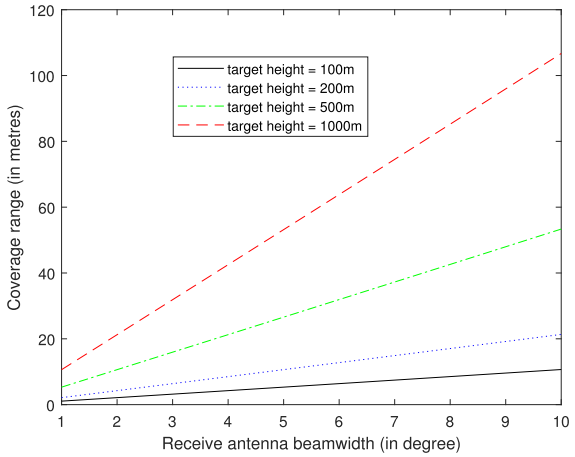

FIGURE 7. Coverage range versus beamwidth for $\theta = 65^o$.

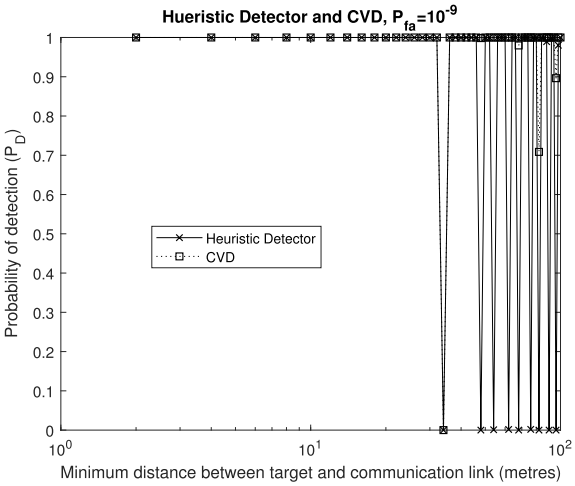

FIGURE 8. Probability of detection for 16QAM for a rectangular target ($a = 0.81m$, $b = 0.64m$) flying along a straight line ($z_G = 500m$, $v_{y_G} = 20\ m/s$, $\theta(t = 0) = 65^o$, $DNR = 10dB$, $N_A = 100,000$, time window = 0.4 second).

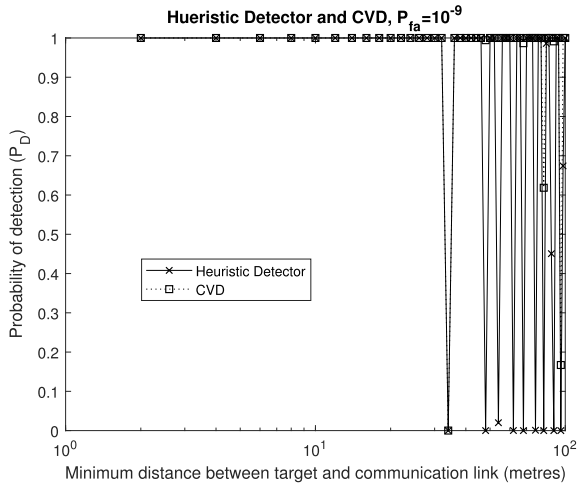

FIGURE 9. Probability of detection for 16QAM for a rectangular target ($a = 0.81m$, $b = 0.64m$) flying along a straight line ($z_G = 500m$, $v_{y_G} = -20m/s$, $\theta(t = 0) = 65^o$, $DNR = 10dB$, $N_A = 100,000$, time window = 0.4 second).

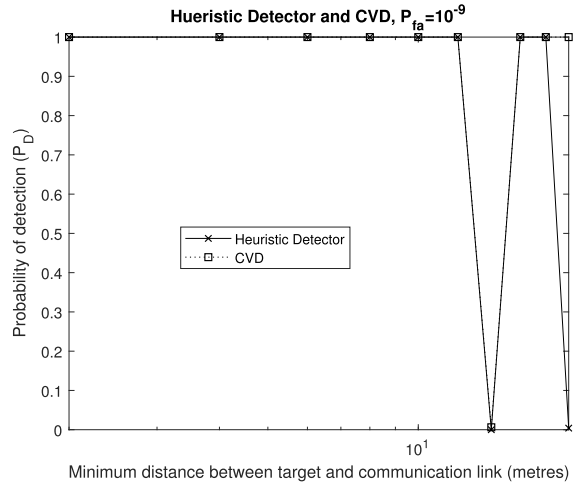

FIGURE 10. Probability of detection for 16QAM for a rectangular target ($a = 0.16m$, $b = 0.13m$) flying along a straight line ($z_G = 100m$, $v_{y_G} = 20\ m/s$, $\theta(t = 0) = 65^o$, $DNR = 10dB$, $N_A = 100,000$, time window = 0.4 second).

$b = 0.13m$ (other parameters are the same as those in Fig. 8) as far as 14 meters. From Figs. 7 to 10, it may be concluded that small targets of size of UAVs flying in low height can be detected by the heuristic detector as long as they are within the beamwidth of the receive antenna, assuming that the beamwidth is as narrow as that used in broadband satellite communications.

D. MULTIPLE SATELLITE LINKS

For a sky fence consisting of multiple ground stations and multiple satellites, thorough Monte Carlo simulations would be quite sophisticated. Instead a simplistic scenario will be considered to gain necessary insights. Let the distance between adjacent ground stations be S meters. From Section V-C, given that a small target flies within the narrow beamwidth of a ground receive antenna, the probability of detection is close to 1. Assume that the track of the target is uniformly distributed on a flat plane parallel to the ground. Then from (14), if the target crosses one link between a satellite and a ground receiver, the probability of detection $P_D \approx \frac{2L}{S} \geq \frac{h\alpha}{S}$. If the target crosses K links, then the probability of detection is given by

$$P_D^K = 1 - (1 - P_D)^K \approx 1 - \left(1 - \frac{h\alpha}{S}\right)^K. \quad (15)$$

For an antenna beamwidth of 3.5^o, Fig. 11 shows the probability of detection v.s. the number of links crossed by a target of 500 meters height for $S = 500, 800, 1,000,$ and $1,500$ meters. It can be seen that the closer the distance between ground stations or the larger the number of links crossed, the better the probability of detection. As an example, if the target crosses about 34 links, a probability of detection of about 50 per cent can be achieved for $S = 1,500$ meters. Fig. 12 shows the probability of detection v.s. the number of links crossed by a target of 100 meters

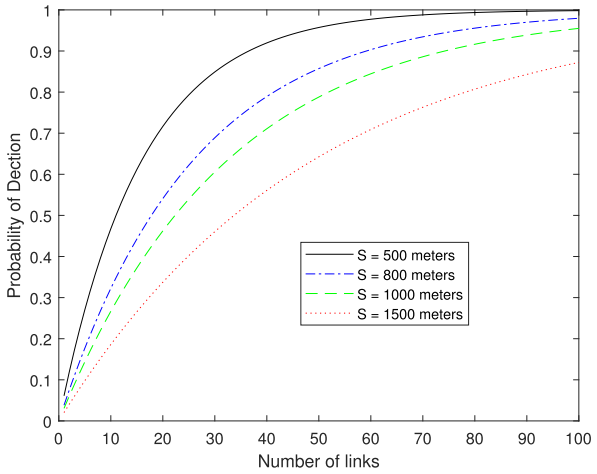

FIGURE 11. Probability of detection with multiple ground stations ($h = 500m$, $\alpha = \frac{3.5\pi}{180}$).

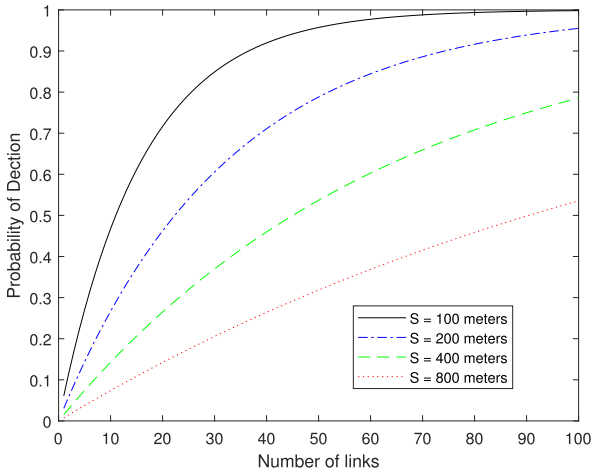

FIGURE 12. Probability of detection with multiple ground stations ($h = 100m$, $\alpha = \frac{3.5\pi}{180}$).

height for $S = 100, 200, 400$, and 800 meters. It can be seen that if the target crosses about 45 links, a probability of detection of about 50 per cent can be achieved for $S = 400$ meters. Note that during the flyover of one ground station, a target may cross multiple links (particularly if the satellite and the target move in the opposite direction, or the target flies slowly), thereby to cross about 45 links the target may only need to fly over a few ground stations. It is worth to mention that, for LEO satellite mega-constellation, at any time multiple satellites are often visible to a ground station. As an example, for Starlink, the number of LEO satellites within the line of sight of a ground station above the minimum required satellite elevation angle is more than 20 for most places on the Earth [29], albeit some of the satellites may not beam down communication signals when the target is crossing the link. However the beacon signals (i.e., single tone signals for tracking Doppler frequency of LEO satellites) are often available [23], [27]), which may be exploited by the sky fence envisioned.

VI. CONCLUSION

A heuristic detector has been proposed for FS radar with opportunistic signals from broadband LEO based communication systems, which requires neither the availability of the direct signal nor the parameters of the flying target. The ROC analysis was carried out with a simple signal model of signal plus noise, which had been shown to be consistent with simulation results. Based on the ROC analysis, it has been shown that for small targets flying with the narrow beamwidth of the ground receive antenna of broadband satellite communication systems, same as the traditional crystal video detector, the proposed heuristic detector can achieve very high probability of detection but with much lower complexity. The application of the proposed detector in a sky fence (i.e., a network of links from multiple LEO satellites to multiple ground receivers across diverse locations) have also been analyzed, demonstrating its potential for UAV detection.

APPENDIX
PROOF THAT THE MATCHED FILTER BASED DETECTOR HAS THE SAME ROC AS THE CRYSTAL VIDEO DETECTOR

Let $X > 0$ be a test statistics for the matched filter based detector. If $X < T_1$, where T_1 is a threshold, it is deemed $\mathcal{H}_0$; otherwise, it is deemed $\mathcal{H}_1$. The cdfs of X under $\mathcal{H}_0$ and $\mathcal{H}_1$ are $F_{\mathcal{H}_0}(x)$ and $F_{\mathcal{H}_1}(x)$, respectively. As a result, $P_{fa} = 1 - F_{\mathcal{H}_0}(T_1)$ and $P_D = 1 - F_{\mathcal{H}_1}(T_1)$, and the ROC is given by

$$P_D = 1 - F_{\mathcal{H}_1}\left(F^{-1}_{\mathcal{H}_0}(1 - P_{fa})\right). \tag{16}$$

In the CVD [21], $Y = \sqrt{X}$ is used as the test statistics. The cdf of Y under $\mathcal{H}_0$ is given by

$$\begin{aligned} P(Y < y; \mathcal{H}_0) &= Prob(\sqrt{X} < y; \mathcal{H}_0) \\ &= Prob(X < y^2; \mathcal{H}_0) \\ &= F_{\mathcal{H}_0}(y^2). \end{aligned} \tag{17}$$

The cdf of Y under $\mathcal{H}_1$ is given by

$$\begin{aligned} P(Y < y; \mathcal{H}_1) &= Prob(\sqrt{X} < y; \mathcal{H}_1) \\ &= Prob(X < y^2; \mathcal{H}_1) \\ &= F_{\mathcal{H}_1}(y^2). \end{aligned} \tag{18}$$

Given a threshold T_2 to select hypothesis $\mathcal{H}_0$ or $\mathcal{H}_1$, then $P_{fa} = 1 - F_{\mathcal{H}_0}(T_2^2)$ and $P_D = 1 - F_{\mathcal{H}_1}(T_2^2)$, from which we can obtain the same ROC as (16).

REFERENCES

[1] Australia Government Civil Aviation Safety Authority (CASA). *The RPAS and AAM Strategic Regulatory Roadmap*. Accessed: Jan. 30, 2024. [Online]. Available: https://www.casa.gov.au/rpas-aam-roadmap

[2] S. O. Ajakwe, D. S. Kim, and J. M. Lee, "Drone transportation system: Systematic review of security dynamics for smart mobility," *IEEE Internet Things J.*, vol. 10, no. 16, pp. 14462–14482, Aug. 2023.

[3] International Civil Aviation Organization (ICAO). *Unmanned Aircraft Systems Traffic Management (UTM)A Common Framework with Core Principles for Global Harmonization, Edition 4*. Accessed: Jan. 30, 2024. [Online]. Available: https://www.unmannedairspace.info/emerging-regulations/icao-releases-edition-4-of-utm-framework-to-facilitate-harmonisation-between-utm-and-atm/

[4] M. Stevens and E. Atkins, "Geofence definition and deconfliction for UAS traffic management," *IEEE Trans. Intell. Transp. Syst.*, vol. 22, no. 9, pp. 5880–5889, Sep. 2021.

[5] M. A. Khan, H. Menouar, A. Eldeeb, A. Abu-Dayya, and F. D. Salim, "On the detection of unauthorized drones—Techniques and future perspectives: A review," *IEEE Sensors J.*, vol. 22, no. 12, pp. 11439–11455, Jun. 2022.

[6] S. Park, H. T. Kim, S. Lee, H. Joo, and H. Kim, "Survey on anti-drone systems: Components, designs, and challenges," *IEEE Access*, vol. 9, pp. 42635–42659, 2021.

[7] H. Griffiths, "Early history of bistatic radar," in *Proc. Eur. Radar Conf. (EuRAD)*, London, U.K., Oct. 2016, pp. 253–257.

[8] C. Hu, C. Liu, R. Wang, L. Chen, and L. Wang, "Detection and SISAR imaging of aircrafts using GNSS forward scatter radar: Signal modeling and experimental validation," *IEEE Trans. Aerosp. Electron. Syst.*, vol. 53, no. 4, pp. 2077–2093, Aug. 2017.

[9] M. Contu, A. De Luca, S. Hristov, L. Daniel, A. Stove, M. Gashinova, M. Cherniakov, D. Pastina, P. Lombardo, A. Baruzzi, and D. Cristallini, "Passive multifrequency forward-scatter radar measurements of airborne targets using broadcasting signals," *IEEE Trans. Aerosp. Electron. Syst.*, vol. 53, no. 3, pp. 1067–1087, Jun. 2017.

[10] R. S. A. R. Abdullah, S. A. Musa, N. E. A. Rashid, A. Sali, A. A. Salah, and A. Ismail, "Passive forward-scattering radar using digital video broadcasting satellite signal for drone detection," *Remote Sens.*, vol. 12, no. 18, p. 3075, Sep. 2020.

[11] I. Theodorou, C. Ilioudis, C. Clemente, M. Vasile, and J. Soraghan, "SISAR imaging for space debris based on nanosatellites," *IET Radar, Sonar Navigat.*, vol. 14, no. 8, pp. 1192–1201, Aug. 2020.

[12] D. Huang, "Doppler analysis of forward scattering radar with opportunistic signals from LEO satellites," *IEEE Access*, vol. 10, pp. 109597–109608, 2022.

[13] D. D. Huang, "Passive positioning of flying object with microwave signals from LEO satellites: Concept and preliminary simulation results," *IEEE Access*, vol. 9, pp. 14640–14648, 2021.

[14] M. Gashinova, L. Daniel, V. Sizov, E. Hoare, and M. Cherniakov, "Phenomenology of Doppler forward scatter radar for surface targets observation," *IET Radar, Sonar Navigat.*, vol. 7, no. 4, pp. 422–432, Apr. 2013.

[15] J. Robie, A. Famili, and A. Stavrou, "Revisiting the spaceborne illuminators of opportunity for airborne object tracking," *Computer*, vol. 56, no. 1, pp. 82–92, Jan. 2023.

[16] J. Robie, A. Famili, and A. Stavrou, "Receiver density analysis for high probability detection of forward scattered airborne signals," in *Proc. Int. Conf. Electr., Comput. Energy Technol. (ICECET)*, Prague, Czech Republic, Jul. 2022, pp. 1–6.

[17] *Space Fence*. Accessed: Jan. 30, 2024. [Online]. Available: https://www.lockheedmartin.com/en-us/products/space-fence.html

[18] G. Muntoni, G. Montisci, T. Pisanu, P. Andronico, and G. Valente, "Crowded space: A review on radar measurements for space debris monitoring and tracking," *Appl. Sci.*, vol. 11, no. 4, p. 1364, Feb. 2021.

[19] J. Glaser, "Bistatic RCS of complex objects near forward scatter," *IEEE Trans. Aerosp. Electron. Syst.*, vol. AES-21, no. 1, pp. 70–78, Jan. 1985.

[20] X. Shen and D. Huang, "Forward scatter shadow ratio: Concept and its application in shadow profile retrieval," *IEEE Access*, vol. 11, pp. 77147–77162, 2023.

[21] N. Ustalli, P. Lombardo, and D. Pastina, "Detection performance of a forward scatter radar using a crystal video detector," *IEEE Trans. Aerosp. Electron. Syst.*, vol. 54, no. 3, pp. 1093–1114, Jun. 2018.

[22] C. Hu, V. Sizov, M. Antoniou, M. Gashinova, and M. Cherniakov, "Optimal signal processing in ground-based forward scatter micro radars," *IEEE Trans. Aerosp. Electron. Syst.*, vol. 48, no. 4, pp. 3006–3026, Oct. 2012.

[23] R. Blázquez-García, D. Cristallini, M. Ummenhofer, V. Seidel, J. Heckenbach, and D. O'Hagan, "Capabilities and challenges of passive radar systems based on broadband low-Earth orbit communication satellites," *IET Radar, Sonar Navigat.*, vol. 18, no. 1, pp. 78–92, Jan. 2024.

[24] O. K. Ersoy, *Diffraction, Fourier Optics and Imaging*. Hoboken, NJ, USA: Wiley, 2006.

[25] I. Ali, N. Al-Dhahir, and J. E. Hershey, "Doppler characterization for LEO satellites," *IEEE Trans. Commun.*, vol. 46, no. 3, pp. 309–313, Mar. 1998.

[26] M. F. Mesiya, *Contemporary Communication Systems*. New York, NY, USA: McGraw-Hill, 2013.

[27] T. E. Humphreys, P. A. Iannucci, Z. M. Komodromos, and A. M. Graff, "Signal structure of the Starlink Ku-band downlink," *IEEE Trans. Aerosp. Electron. Syst.*, vol. 59, no. 5, pp. 6016–6030, Oct. 2023.

[28] S. Kay, *Fundamentals of Statistical Processing, Volume 2: Detection*, vol. 2. Upper Saddle River, NJ, USA: Prentice-Hall, 1998.

[29] I. del Portillo, B. G. Cameron, and E. F. Crawley, "A technical comparison of three low Earth orbit satellite constellation systems to provide global broadband," *Acta Astronautica*, vol. 159, pp. 123–135, Jun. 2019.

[30] D. Huang, "A heuristic detector for forward scatter radar with opportunistic signals from LEO satellites," in *Proc. IET Int. Radar Conf. (IRC)*, Chongqing, China, 2023, pp. 1–7.

DEFENG (DAVID) HUANG (Senior Member, IEEE) received the B.E.E.E. and M.E.E.E. degrees in electronic engineering from Tsinghua University, Beijing, China, in 1996 and 1999, respectively, and the Ph.D. degree in electrical and electronic engineering from Hong Kong University of Science and Technology (HKUST), Hong Kong, in 2004.

In 2005, he joined as a Lecturer with the School of Electrical, Electronic, and Computer Engineering, The University of Western Australia (UWA). He has been a Professor with the School of Electrical, Electronic, and Computer Engineering, since 2011. Before joining UWA, he was a Lecturer at Tsinghua University. He served as an Editor for the IEEE Wireless Communications Letters, from 2011 to 2015, and IEEE Transactions on Wireless Communications, from 2005 to 2011; and an Editorial Assistant for IEEE Transactions on Wireless Communications, from 2002 to 2004.